Jürgen Sachs, Ralf Herrmann:

M-sequence-based ultra-wideband sensor network for vitality monitoring of elders at home

URN: urn:nbn:de:gbv:ilm1-2015200048

Source:	IET Radar, Sonar & Navigation, 9 (2015), 2, p. 125 - 137.
DOI:	10.1049/iet-rsn.2014.0214
Print ISSN	1751-8784
Online ISSN	1751-8792
URL:	http://dx.doi.org/10.1049/iet-rsn.2014.0214

Published in IET Radar, Sonar and Navigation
Received on 4th May 2014
Revised on 7th November 2014
Accepted on 6th December 2014
doi: 10.1049/iet-rsn.2014.0214

ISSN 1751-8784

M-sequence-based ultra-wideband sensor network for vitality monitoring of elders at home

Jürgen Sachs, Ralf Herrmann

Electronic Measurement Engineering Group, Technische Universität Ilmenau, Ilmenau, Germany
E-mail: juergen.sachs@tu-ilmenau.de

Abstract: The western societies are increasingly faced with the challenges of enabling a self-determined and safe life for a growing number of elderly people. Remote monitoring of vitality is an important tool for health risk mitigation but many of the current methods either deliver only infrequent information or require conscious cooperation of the senior. The authors propose an ultra-wideband (UWB) radio sensor network based on M-sequence technology specifically designed for the vitality monitoring of persons living alone. It uses the frequency band in the range from 6 to 8.5 GHz (electronic communications committee (ECC)-band), and provides precise localisation, captures breathing motion during rests, can be used for fall detection and allows the extraction of gait features. The sensor network can be installed in common living spaces. It operates continuously in the background without any user interaction. Vitality monitoring by radar sensors is based on motion detection and tracking. This poses some challenges to radar devices because of the harsh multi-path conditions in apartments. This study discusses these challenges, illustrates how to meet them and gives examples for vitality features which can be extracted from UWB-radar data.

1 Introduction

The dramatic demographic change confronts many countries with outstanding social and structural transformations. An ageing society will increasingly affect the financial burden of the health sector, of welfare institutions and retirement funds. Many seniors live alone in their home where they may be unattended over several hours or even days. In the case of an incident (tumbling and fall, heart attack etc.), they are helpless and risk dying or remaining in uncomfortable situations over a long period. Against this background, automatic assistance systems [1] promise help and support for elderly people to live independently in their familiar environment, with relatives, medical and nursing staff being at their disposal, too.

Such assistance systems continuously need input data which provides information about the vitality state and situation of the person being looked after. This data must be captured without violation of privacy and without need for active support from the senior (e.g. carrying a bracelet with sensors or other tags, which would be too demanding for demented people). On the basis of this continuous data stream, the assistance system shall detect abnormal and critical situations of the needy person and autonomously initiate the call for help. Any kind of body motions – the gait, chest movements because of breathing and heartbeat, insomnia as well as the daily routine at home – are expedient indicators of the vitality of a human being. High-resolution, short-range (low power – a thousand times less than a cell phone) radar sensors are able to detect and track such kind of motions remotely, continuously, unobtrusively and without any risks for the monitored person.

The classical concept of motion detection by radar is the Doppler radar. It applies a time harmonic wave of constant frequency for sounding the scenario under test while recording all phase variations of the backscattered signals. In the case a target is moving at a constant radial speed, this phase changes linearly in time, which leads to the creation of the well-known Doppler frequency. Supposing low additive and phase noise, a Doppler sensor is able to register very sensitively small geometric variations within a scenario under test. Owing to the lack of range resolution, its output signal represents a superposition of the motion of all objects within the beam of the radar antenna. Nevertheless, one is able to separate various types of motions if their time histories are sufficiently different [2–4]. However, in many cases, (e.g. the supervision of a strictly geometrically limited area or the motion separation of several moving objects) the simple Doppler sensor often fails, and, thus, is not able to localise the person.

In such cases, a sensor principle may help which provides both high range as well as motion resolution. Ultra-wideband (UWB) radar fulfils such condition while providing additionally the good penetration of many substances if it works in the baseband (i.e. below a few gigahertz (GHz)).

In what follows, we will estimate the performance of the UWB radar to detect the motion of a target and its position. First, we will discuss some aspects of the detection limits of moving targets for an idealised indoor scenario. Most publications in which those aspects are dealt with only respect signal corruptions by additive amplitude noise. This is, however, far from reality in a measurement environment containing strong static reflectors, as it is the case in typical apartments. Radar devices are also subjected to random

'temporal noise' (jitter) which creates time-dependent extra noise and false targets. This degrades or even prevents the detection of the wanted targets. Furthermore, we will briefly introduce sensing devices which respect the observations made in the second paragraph. Next, we will discuss some aspects of UWB-scattering from a human being. Finally, we will give some examples of vitality features gathered in the laboratory as well as during a month-long measurement campaign in the apartments of seniors. For the purpose of vitality feature extraction, we split up the motion of a human into three levels:

- Coarse motion – global motion of the torso.
- Fine motion – motion of the limbs.
- Micro-motion – respiration, heartbeat and vestibular oscillations.

2 Indoor target detection

2.1 Radar signal modelling

Fig. 1 depicts a simplified propagation scenario under indoor conditions. For the purpose of a better illustration, we consider a simple pulse-radar emitting periodically (time interval ΔT) sub-nanosecond baseband pulses. The goal is to detect the moving object, to track its position and to register any other variations such as the body shape. The antenna has only low directivity, thus permitting a large solid angle of space to be surveyed. This approach requires two or more radar sensors in order to provide the target position by trilateration as considered, for example, in [5, 6], which we will not discuss here in detail. Instead, we are interested in finding out how the backscatter signal of the desired target can be extracted from the mixture of radar signals and what phenomena affects the detection performance. In our signal model, we assume the electromagnetic interactions to run in a much shorter time than the temporal variations of the scenario under test. This allows us to consider the scenario as locally stationary during the capturing of a single radar response so that the signals involved may be expressed as functions of two independent time variables. These are t (the propagation or fast time representing the time scale within which the electromagnetic interactions take place) and $T = n\Delta T$ (the observation or slow time referring to the time scale for which the temporal variation of the scenario under test becomes notable). As can be seen from Fig. 1, the received signal $b(t, T)$ at observation time T is composed of many reflections $b_1(t, T)$, $b_2(t, T)$, $b_3(t, T)$ of static and moving objects

$$b(t,\ T) = b_1(t) + b_2(t,\ T) + b_3(t,\ T) \tag{1}$$

As we have assumed a short stimulation pulse, $b(t, T)$ represents the total impulse response function (IRF) of the scenario under test. We have disregarded multiple reflections between the objects in (1) because their amplitude is usually much smaller than the first reflections. We have included two types of static objects. In the first case, the scattering signal $b_1(t, T) = b_1(t)$ does not vary with observation time T since the moving target does not influence its illumination. For the second type, exemplified by the wall reflection $b_3(t, T)$, the backscattering depends on T (even if the scattering object is static) since the illumination is modulated by the target if it approaches the position of the dashed circle in Fig. 1*a*.

The signal $b_2(t, T)$ refers to the moving target. This is exactly what we are interested in. Hence, the first step of the radar processing must be to extract it from the measurements $b(t, T)$. Owing to the variable distance between moving target and antenna, the time position t_P (i.e. the roundtrip time) of $b_2(t, T)$ is shifted as a function of T. Unfortunately, the time position t_P of a pulse may be neither defined uniquely nor it is independent of the pulse shape [7]. Fig. 4 illustrates the variations of the backscattering of a human body as a function of the aspect angle. As we can observe, it will hardly be possible to exactly link body position and roundtrip time. We may estimate t_P either from the location of the pulse peak, the crossing of a threshold or any centre of gravity $t_{P,n}$ [8].

$$t_{P,n}(T) = \frac{\int t\left|b_2(t,\ T)\right|^n dt}{\int \left|b_2(t,\ T)\right|^n dt};\quad n = 1,\ 2,\ 3,\ \ldots \tag{2}$$

For $n = 2$, we call $t_{P,2}$ the energetic centre of the pulse.

For a walking human, the aspect angle and his body geometry (e.g. the arrangement of the limbs) will vary over the time T. This leads to a time-variant pulse shape of the return signal. Since, as we have seen, the roundtrip time estimation depends on the pulse shape, the accuracy of the t_P – estimation will be less dependent on the radar performance (UWB radar supposed) than on the geometric variability of the target. To obtain an impression of walking-induced pulse shape variations, the function $F(T_1, T_2)$ can be used

$$F\left(T_1,\ T_2\right) = \frac{\left\| C_{T_1, T_2}(\tau)\right\|_\infty^2}{C_{T_1, T_1}(0) C_{T_2, T_2}(0)} \le 1 \tag{3}$$

which is borrowed from the fidelity [8]. It indicates the strength and the temporal pattern of the fluctuations of the target reflections. Here, $C_{T_1 T_2}(\tau) = \int b_2\left(t,\ T_1\right) b_2\left(t+\tau,\ T_2\right) dt$ represents the correlation function of the target reflection at T_1 and T_2. If $F(T_1, T_2)$ approaches one, the roundtrip times $t_P(T_1)$ and $t_P(T_2)$ refer to identical postures and aspect angles of, for example, a walking person. Hence, $t_P(T_2) - t_P(T_1)$ gives a measure of the actual displacement of the body. If $F(T_1, T_2)$ is <1, then $t_P(T_2) - t_P(T_1)$ is dependent on both the body displacement and the variations of the posture or the aspect angle.

Fig. 5 in Section 4 illustrates the UWB signals for a simple but real scenario in which the different signal components (for demonstration purposes) do not overlap. However, under the strong multi-path conditions in an apartment, the typically dominant signal component $b_1(t)$ will cover the desired signal $b_2(t)$, as symbolised in Fig. 1*b*.

2.2 Extraction of moving target

To extract the desired signal $b_2(t, T)$, one usually subtracts from the measurements $b(t, T)$ the signal $b_e(t)$ which we gain from measurements in the absence of the person (i.e. $b_2(t) = 0$). This leads to the signal $c(t, T)$, which represents the time-variant part of the scenario IRF $b(t, T)$

$$c(t,\ T) = b(t,\ T) - b_e(t) = b_2(t,\ T) - \widehat{b}_3(t,\ T) \tag{4}$$

It is used for target detection, roundtrip time estimation and the extraction of further target features. It consists of the

doi: 10.1049/iet-rsn.2014.0214

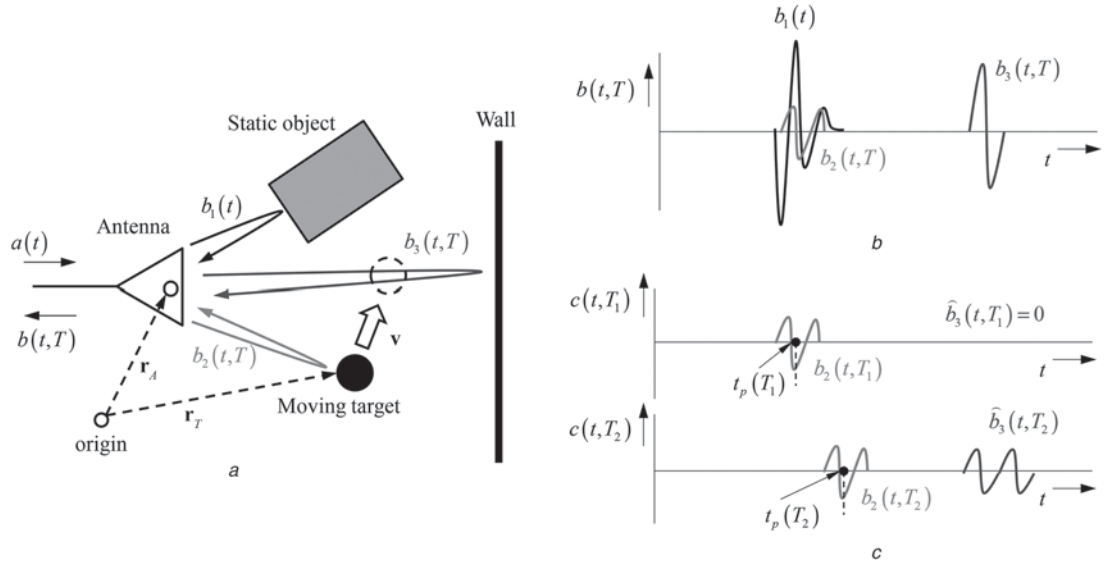

Fig. 1 *Idealised indoor radar scenario*

a Simplified (mono-static) radar scenario for indoor propagation
b Expected radar signals from each object
c Signal components of the captured data after static background removal for two different states of the test scenario (T_1 is the target at the 'black' position and T_2 is the target at the dashed position). ($\mathbf{r}_A$, $\mathbf{r}_T$ are the position vectors of antenna and target, v is the target speed, t_p is the roundtrip time of the target)

desired target reflection $b_2(t, T)$ and the signal $\hat{b}_3(t, T)$ provoked by the target if it shadows the wall illumination (compare Fig. 1*c*). Hence, we call $\hat{b}_3(t, T)$ the shadow signal. With respect to the propagation time t, the shadow signal always appears behind the target so that the roundtrip time of the target $t_P(T)$ represents the position of the first pulse in $c(t, T)$. However, it should be noted that the shadow signal can be stronger than that of the target under certain circumstances.

The signal $b_e(t)$ is often assigned as background corresponding to the time-invariant part of the total IRF $b(t, T)$. According to our scenario model, we may express it as

$$b_e(t) = b_1(t) + b_3(t) \tag{5}$$

if the apartment is in a stationary state. In that case, $b_e(t)$ does not depend on the observation time; that is why we neglect T in (5). A second, more practical way (without prior exclusion of the target) to find $b_e(t)$ is to use the original measurement data $b(t, T)$ and to suppress $b_2(t, T)$ by averaging the data along the T direction within a sliding window of an appropriate duration T_a. This is equivalent to the stacking of $P = T_a/\Delta T$ consecutive measurements

$$b_e(t,T)=\overline{b(t,T)}\big|_{T_a}=\frac{1}{T_a}\int_{T-T_a}^{T_a} b(t,\tau)\mathrm{d}\tau=\frac{1}{T_a}b(t,T)*_T\mathrm{rect}\left(\frac{T}{T_a}\right)$$

$$b_e(t,n\Delta T)=\frac{1}{P}\sum_{p=n-P}^{n-1} b(t,p\Delta T)\ \text{with}P=\frac{T_a}{\Delta T} \tag{6}$$

rect(···) is the rectangular function (or other low pass) $*_T$ is the convolution with respect to T.

Now, the background signal is slightly dependent on the observation time so that it can compensate for minor temporal variations of the apartment geometry (e.g. displacement of a chair, opening a door etc.). This method presupposes, of course, that the person is walking around in such a way that their backscattering $b_2(t, T)$ is sufficiently suppressed by the averaging filter. If the subject is in a resting position or a duration approaching T_a or even longer, their body reflection becomes part of the background and will vanish from $c(t, T)$. However, because of breathing and heartbeat, the human body will never be absolutely static so that minor modulations of the radar signal remain in $c(t, T)$. They may relate, for example, to respiration and heartbeat-induced motions of the chest (see Fig. 9 in Section 5. for an example).

2.3 Random perturbations

In what follows, we are investigating how random fluctuations of the radar device limit the detection performance of the moving target. However, for the sake of conciseness, we leave the shadow signal out of consideration (i.e. $b_3(t, T) = 0$). Random fluctuations appear in both amplitude and time axis, whereas the latter is ignored in most publications of indoor UWB-radar applications. They are generally denoted as additive noise $n(t, T) \sim N(0, \sigma_n^2)$ and sampling jitter $\Delta\tau_j(t, T) \sim N\left(0, \varphi_j^2\right)$. In properly designed sensing devices, they can be assumed to be Gaussian distributed with variance σ_n^2 and φ_j^2, ergodic as well as mutually uncorrelated and independent. The related probability density functions (PDFs) are assigned as $p_n(b)$ for the additive noise and $p_{\Delta\tau_j}(t)$ for the sampling jitter. We can model the received signal by a random process as (see (7) at the bottom of the next page).

The second line in the equation comes from Taylor-series expansion, which we terminated after the first term since the jitter was supposed to be small. In (7), b represents a deterministic variable, $\underset{\sim}{b}$ is a random variable and $\dot{b}(t, T)$ denotes the first derivative with respect to the propagation time t. The jitter effect on the captured additive noise is summarised by the symbol $\underset{\sim}{n}_j(t, T)$. Since the additive noise

was assumed to be ergodic, the time of data capturing has no impact on the statistical noise properties and hence it holds for the variance $\mathrm{var}\{\underset{\sim}{n}_j(t,\ T)\} = \mathrm{var}\{\underset{\sim}{n}(t,\ T)\} = \sigma_n^2$.

Target detection and characterisation is based on $c(t,\ T)$ from which we estimate the expected value and the variance in what follows. For that purpose, we consider the random process $\underset{\sim}{c}(t,\ T) = \left[\, c_1(t,\ T) \quad c_2(t,\ T) \quad \cdots \ c_n(t,\ T) \cdots \right]$ that is built from numerous realisations $c_n(t,\ T)$. The expected value and the variance are given by

$$E\{\underset{\sim}{c}(t,\ T)\} = \lim_{N\to\infty} \frac{1}{N} \sum_{n=1}^{N} c_n(t,\ T)$$

$$\mathrm{var}\{\underset{\sim}{c}(t,\ T)\} = E\{\underset{\sim}{c}^2(t,\ T)\} - (E\{\underset{\sim}{c}(t,\ T)\})^2 \tag{8}$$

Related to (4), we first need the background $\underset{\sim}{b}_e(t,\ T)$ in order to obtain $\underset{\sim}{c}(t,\ T)$. As shown in (6), the background signal is usually gained from an averaging process along the T-axis. That procedure largely suppresses the noise and removes the moving target from the data (i.e. $\overline{b_2(t,\ T)}|_{T_a} \simeq 0$). Respecting additive noise and jitter (see the annex for analysis of the jitter effect), we can write the expected value and variance of the background signal as (* convolution with respect to t)

$$\begin{aligned} E\{\underset{\sim}{b}_e(t,\ T)\} &= E\{\overline{\underset{\sim}{b}(t,\ T)}|_{T_a}\} \\ &\simeq E\{\overline{(b_1(t + \Delta\,\underset{\sim}{\tau}_j(t),\ T) + \underset{\sim}{n}_j(t,\ T))}|_{T_a}\} = p_{\Delta\tau_j}(t) * b_1(t) \\ \mathrm{var}\{\underset{\sim}{b}_e(t,\ T)\} &= \mathrm{var}\{\overline{\underset{\sim}{b}(t,\ T)}|_{T_a}\} \\ &= \frac{1}{P}(b_1^2(t) * p_{\Delta\tau_j}(t) - (b_1(t) * p_{\Delta\tau_j}(t))^2 + \sigma_n^2); \\ \text{with } P &= \frac{T_a}{\Delta T} \end{aligned} \tag{9}$$

and for the time-variant IRF $\underset{\sim}{c}(t,\ T)$, we finally obtain (10) and (11) which tell us that the jitter 'brings back' the static objects into the signal $c(t,\ T)$ that was initially created with the aim of eliminating the static reflections (compare (4)). In (10) and (11), we supposed that the strength of static scatterers dominates that of the moving target. From both equations, we can observe that jitter provokes false targets and extra noise, which are located at the roundtrip time of any strong reflecting static object and which are independent of the observation time T.

To perform a reliable detection, the peak value of the target response $\left\| b_2(t,\ T) \right\|_\infty$ must sufficiently exceed the values of the 'false target' $\ddot{b}_1(t)\varphi_j^2/2$ as well as the standard deviation of the overall noise $\sqrt{\dot{b}_1^2(t)\varphi_j^2/P + \sigma_n^2}$. Hence, in the case of a jitter-prone UWB-sensor, the detection performance for the moving target degrades if its roundtrip time comes close to the roundtrip time of any static object which is located within the antenna beam.

3 Sensor devices

In conclusion from (10) and (11), we are forced to apply UWB-sensor concepts for indoor measurements which are robust against noise and jitter and which suppress the generation of 'false targets' and time-dependent noise in order to achieve high sensitivity and detection reliability. As comprehensively discussed in [8, 9], UWB sensors based on the utilisation of pseudo-noise signals, for example, as M-sequences, are well suited for the intended kind of application since they are designed for low jitter generation, high noise suppression, and, in addition, they prevent the creation of false targets and time-dependent noise. In [10], a short overview of the current state of development is given. Fig. 2 shows some devices which we have used for the measurements that are discussed in the following paragraphs.

The device corresponding to Fig. 2*c* represents a prototype of a cost-efficient implementation of the M-sequence principle designed for the upper European UWB band (6–8.5 GHz). It is designed for vital data capturing of assisted accommodation as discussed in Section 5. Its block

$$\begin{aligned} \underset{\sim}{b}(t,\ T) &= b\left(t + \Delta\underset{\sim}{\tau}_j(t),\ T\right) + \underset{\sim}{\tau}_j\left(t + \Delta\,\underset{\sim}{\tau}_j(t),\ T\right) \\ &\simeq b(t,\ T) + \underbrace{\dot{b}(t,\ T)\Delta\,\underset{\sim}{\tau}_j(t)}_{\text{signal dependent noise term}} + \underset{\sim}{n}_j(t,\ T) \\ &\simeq b_1(t,\ T) + b_2(t,\ T) + \left(\dot{b}_1(t,\ T) + \dot{b}_2(t,\ T)\right)\Delta\,\underset{\sim}{\tau}_j(t) + \underset{\sim}{n}_j(t,\ T) \end{aligned} \tag{7}$$

$$E\{\underset{\sim}{c}(t,\ T)\} = E\{\underset{\sim}{b}(t,\ T) - \overline{\underset{\sim}{b}(t,\ T)}|_{T_a}\} = \left(\delta(t) - p_{\Delta\tau_j}(t)\right) * b_1(t) + b_2(t,\ T) \simeq \underbrace{\frac{1}{2}\ddot{b}_1(t)\varphi_j^2}_{\text{false target}} + \underbrace{b_2(t,\ T)}_{\text{target}} \tag{10}$$

$$\mathrm{var}\{\underset{\sim}{c}(t,\ T)\} = \frac{1}{P}\left(c^2(t,\ T) * p_{\Delta\tau_j}(t) - \left(c(t,\ T) * p_{\Delta\tau_j}(t)\right)^2 + \sigma_n^2\right) + \sigma_n^2 \simeq \underbrace{\frac{1}{P}\dot{b}_1^2(t)\varphi_j^2}_{\substack{\text{elevated noise} \\ \text{at position of} \\ \text{static object}}} + \sigma_n^2 \tag{11}$$

doi: 10.1049/iet-rsn.2014.0214

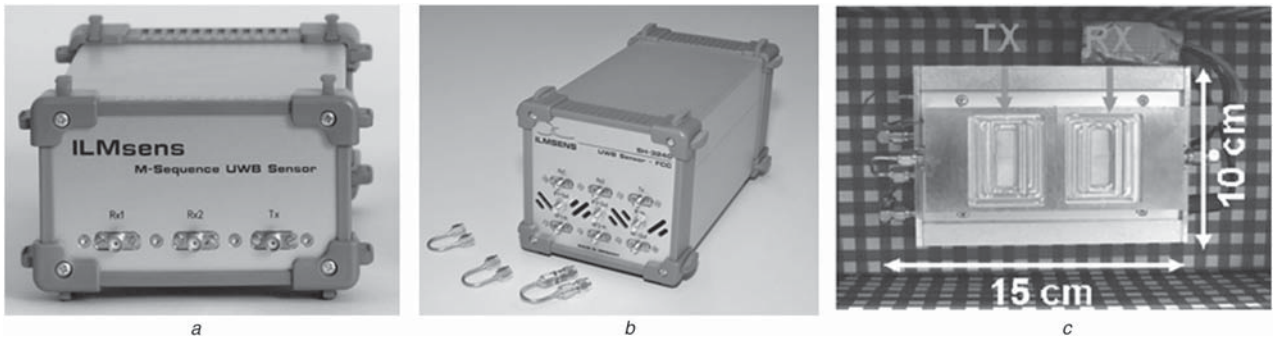

Fig. 2 *UWB devices based on pseudo noise (PN)-sequences for stimulation of the scenario under test*

a Baseband M-sequence device of selectable bandwidth (up to 15 GHz)
b Device operating optionally in the 0–3.5 GHz band (baseband) or the 3.5–10.5 GHz band (FCC-band) or the 6–8.5 GHz band (ECC-band) (courtesy to http://www.ilmsens.com/)
c Modified M-sequence device for the ECC-band with compact stepped cavity horn antennas [11]

schematics and an implementation example are shown in Fig. 3. The transmitter emits the upper sideband of an up-converted M-sequence. The receiver exploits sub-sampling in the third Nyquist zone of the analog to digital converter (ADC) leading to an equivalent sampling rate of $f_{eq} = 3f_0$ which matches well signal and noise bandwidth. The sensor-internal data processing is performed by an field programmable gate array (FPGA). It may execute the synchronous averaging of the captured data, the background removal, the pulse compression and the target detection. It is interesting to note that the fast Hadamard transform can effectively do the pulse compression. It is

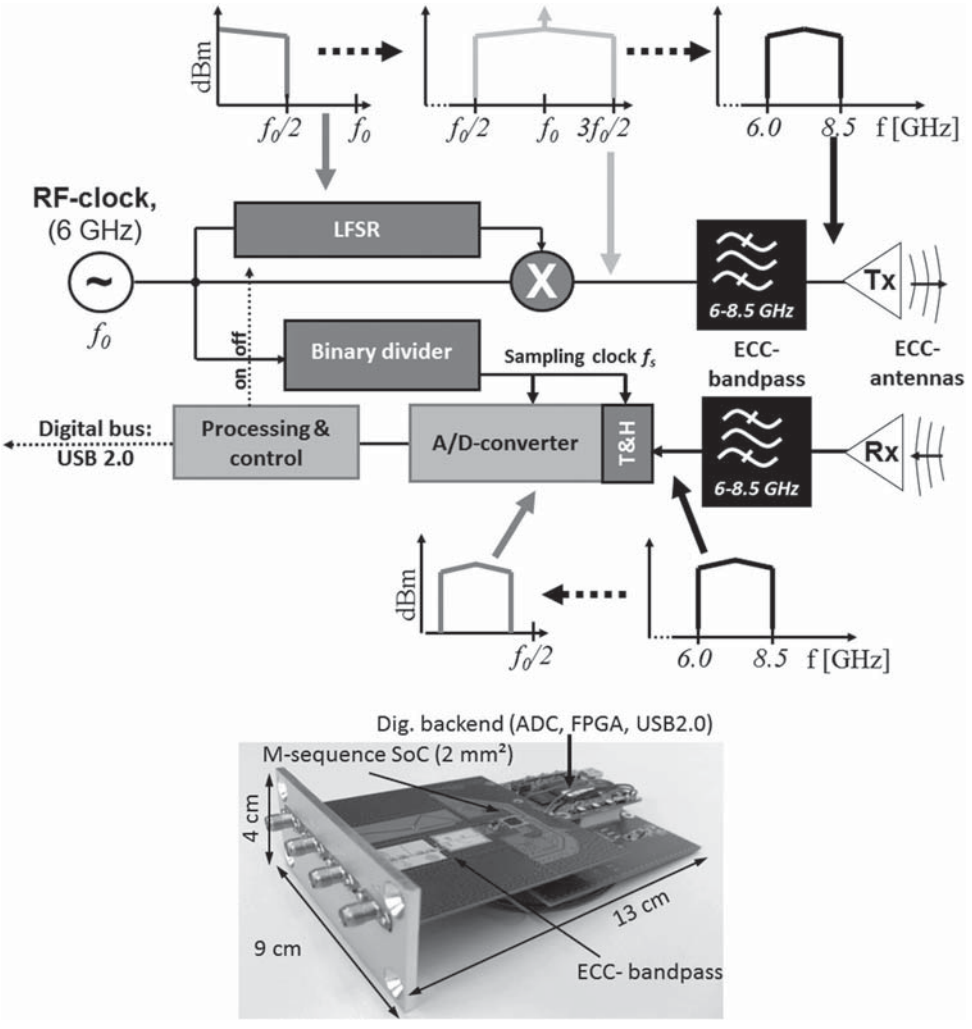

Fig. 3 *Block schematic and test sample implementation of an ECC-band M-sequence sensor*

Stylised spectra in the upper graph represent the occupied frequency bands at the indicated points of the circuit. LFSR is a fast linear feedback shift register that provides the high-speed M-sequence

exclusively based on additions and subtractions of integer numbers, which is well suited for FPGA processing. The code of the actually used M-sequence is respected by a simple permutation of the data sample order which has to be applied before and after the Hadamard transform [8, 12]. However, pulse compression and other steps of processing can also be done on the PC or embedded controller with minor processing burden. Note that all radar signals shown below were already subjected to the pulse compression. The RF-kernel of the ECC-sensor device is built from a single SiGe-ASIC [13]. Thus, apart from the higher sampling rate, the technical implementation complexity is comparable with that of a Doppler- or frequency modulated continuous wave (FMCW)-radar.

The frequency band of the sensor permits operation under UWB radiation rules in Europe and USA. By slightly shifting the RF-clock rate and adapting the band-pass filters, the sensor may also meet the radiation rules of Asian countries [8]. A further advantage of the selected frequency band is its distance to commercial radio services such as GSM, universal mobile telecommunications system (UMTS) or WiFi thereby avoiding jamming of the weak radar signals by the comparatively strong radio emitters of other services.

Beside the frequency band, the length of the M-sequence, the sampling rate and the recording time are essential operational parameters [8]. The length m of the linear feedback shift register (LFSR) controls the period duration of the M-sequence ($T_0 = (2^m - 1)/f_0$) and its feedback structure fixes its code. To avoid time aliasing in the received data, the M-sequence period must be longer than the settling time of the indoor propagation channel. Furthermore, the UWB regulation rules refer to the spectral power in 1 MHz bands. Hence, the M-sequence period should be larger than 1 μs in order to avoid empty 1 MHz bands and to fully exploit the power limit.

The binary divider (length n) fixes the sampling rate $f_s = 2^{-n} f_0$. The selection of its dividing factor depends on a trade-off between measurement speed and receiver efficiency against energy consumption and costs of the digital components.

The recording time T_R denotes the duration to capture the complete set of data samples for one impulse response including synchronous averaging. $T_R = K(2^m - 1)/f_s$ depends on the duration of the M-sequence, the sampling rate f_s and the stacking number K (synchronous averages; do not confuse K with the averaging number P in (6)). A large T_R leads to an improved signal-to-noise ratio of the captured signal [10]. However, the dynamic of the test scenario will limit the duration of the recording. If one wants to set the recording time, two effects must be taken into account. The first one relates to oscillatory motions such as breathing or the heartbeat. This involves complying with the Nyquist theorem in observation time direction, that is, the time interval $\Delta T \geq T_R$ between two consecutive measurements has to meet

$$\Delta T \Omega_{\max} < 1/2 \tag{12}$$

$\Omega_{\max}$ is the highest oscillation rate.

We have typically used ten measurements per second ($\Delta T = 100$ ms) in our experiments, which covers vital signs (e.g. the heartbeat) up to a rate of 200 beats per minute. This should be sufficient under normal conditions but it will not be suited for the registration of ventricular fibrillation (going up to 800 min^{-1}) or harmonics of the heartbeat.

The second effect is connected to continuously moving targets having the range speed (compare Fig. 1*a*) of $v_r = \boldsymbol{v} \cdot (\boldsymbol{r}_T - \boldsymbol{r}_A)/|\boldsymbol{r}_T - \boldsymbol{r}_A|$ ($\cdot$ means dot product of two vectors). This leads to Doppler stretching [8], which provokes de-correlation of the receiving signals if their recording time T_R becomes too long. Therefore, we require

$$\begin{aligned} T_R &< \frac{c_0}{2 \ddot{B} v_{r,\max}} \quad \text{baseband signal} \\ T_R &< \frac{c_0}{(4 \ldots 6) f_0 v_{r,\max}} \quad \text{band-pass signal} \end{aligned} \tag{13}$$

Herein, c_0 is the speed of light, $\ddot{B}$ is the double-sided bandwidth of a baseband signal (used by the device related to Fig. 2*a*) and f_0 is the centre frequency of an UWB-band-pass signal (used by the devices related to Fig. 2*b*, *c*). Note that UWB signals are not simply subjected to a Doppler (frequency) shift and that they are not subjected to Doppler ambiguity. This implies that the range velocity does not constrain the measurement rate. However, higher-order motion components such as acceleration and jerk will require a minimum measurement rate. The proposed rate of ten measurements per second is sufficiently high for walking related acceleration and jerk. In our experiments, we have usually selected $T_R \simeq 3$ ms leading to a maximum target speed of about 3 m/s in the case of ECC-band experiments according to (13). This seems to be appropriate for walking within an apartment. Note, however, that the maximum speed is not only related to the (average) displacement of the body. Instead, it must also respect the motion of the limbs, which may move much faster.

4 Back-scattering of the human body

To obtain some impressions about the reflections from a human body, we have made several experiments with stationary and moving people. Fig. 4 exemplifies the angular dependency of the backscattering in the case of vertically polarised antennas. As we can observe, the strength of the scattering may be quite weak for some aspect angles (e.g. at about ±120°) but for other angles, we may even obtain two reflections (compare Fig. 4*c*). It should, however, be noted that the backscattering response largely depends on the bearing, the arm position and so forth. We can draw three conclusions from these measurements:

- In a sensor network as used in Fig. 7, the detection procedure of an individual UWB-sensor may fail because of an unfavourable aspect angle. Hence, instead on the target, the detector may stick on a false target (see (10) or on a shadow of the target).
- Owing to the strong dependency of the shape of the reflected signal on the body posture, it is difficult, if not impossible, to determine a unique value for the roundtrip time of the whole body. Integral-based methods of roundtrip time estimation (see (2)) equalise a little the influence of the pulse shape onto the pulse position.
- It can be observed – as emphasised by the grey interval of the curve in Fig. 4*c* – that the backscattering fluctuates (irregularly) in time even if the volunteer does their very best to stand motionless. Hence, the absence of such fluctuations in the radar data is a good indicator for unconsciousness of an individual.

doi: 10.1049/iet-rsn.2014.0214

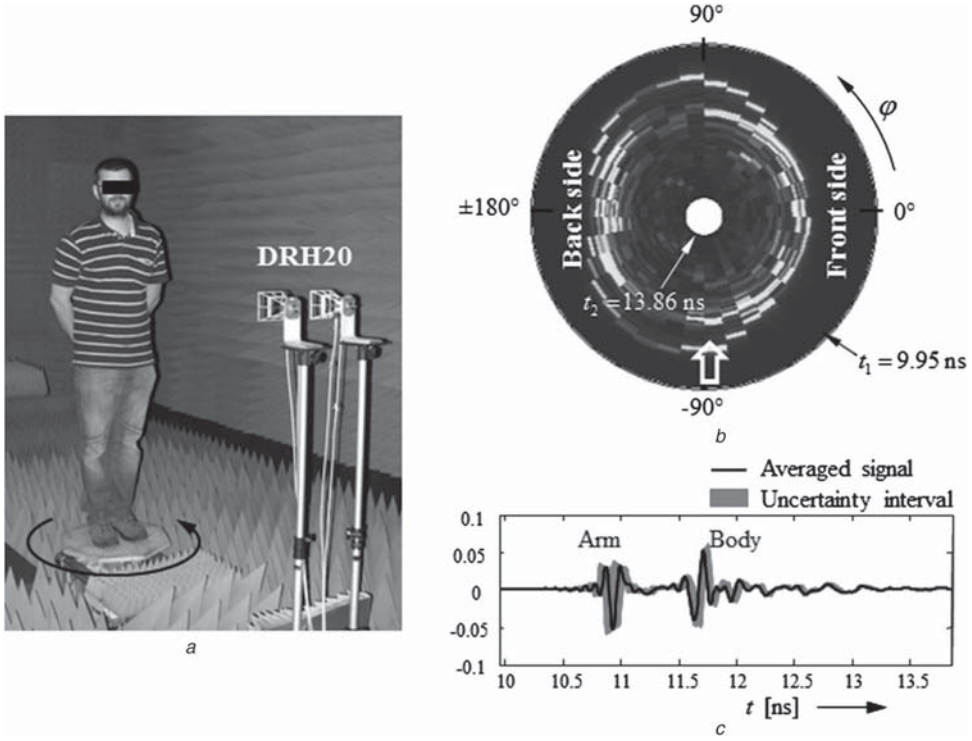

Fig. 4 *UWB-backscattering of a human body*

a Measurement setup with turntable and M-sequence radar (12 GHz bandwidth [14])
b Angle-dependent impulse response (envelope) of a person for vertically polarised waves
c Backscattered signal at $\varphi = -90°$ (see the bold arrow in picture *B*)

A second example deals with two experiments of a walking human (Fig. 5). His backscattering was captured through a brick wall (30 cm thick) and in the presence of a wall at the opposite side in order to demonstrate the performance of background removal and the generation of shadow signals. As the measured data $b(t, T)$ show (Fig. 5*a*), the static objects dominate the radar signals. Moving persons are not visible at all.

In the first experiment, the person was walking on the spot so that the time of flight was constant during the whole measurement. The arms were vigorously agitated. The upper diagram in Fig. 5*b* shows the time-variant IRF $c(t, T)$ after background removal (calculated via (4)). It represents the time variations of the impulse response of the person for illumination of its front side ($\varphi = 0$). A specific pattern of walking becomes visible so that selected features of this pattern can be used to characterise the gait of a person. Via long-term monitoring, one is finally able to detect anomalies which may indicate health and vitality problems of the person under observation. Selection of the best gait features for that purpose is subject of ongoing research. Other data representations beside the time-variant IRF $c(t, T)$ may also be useful for the extraction of appropriate gait features. One is shown in the lower part of Fig. 5*b* that represents the envelope $c_{en}(t, T) = \left|c(t, T) + \mathrm{j}\hat{c}(t, T)\right|$ calculated via the absolute value of the analytic signal ($\hat{c}(t, T) = c(t, T) * (\pi t)^{-1}$-Hilbert transform of $c(t, T)$ in the t-direction). In a further representation, usually referred to as Micro-Doppler signature, the time-variant IRF $c(t, T)$ is subjected to a time-frequency analysis in T direction via short-time Fourier Transform. This leads to a three-dimensional data set, which is also called joint range–time–frequency representation [15]. We do not want to pursue that approach here, because on one hand it increases dramatically the amount of data, and on the other hand all information over the scattering object is already encrypted in the pattern of $c(t, T)$. The interested reader may find a comprehensive overview of Micro-Doppler research in [16].

Figs. 5*c–g* refer to a second experiment in which a person approaches the antenna and then goes back. The gait was relaxed without excessive movement of the arms. In contrast to the first experiment, we now have to deal with the superposition of two types of motion – the global displacement of the body (coarse motion) and the variation of the geometric body structure (fine motion). The radar data cleaned from static background are shown in Fig. 5*c*. We can identify the trace of the target $b_2(t, T)$ and the target shadow $\widehat{b_3}(t, T)$ located at about 70 ns of the propagation time t. A false target at the position of the first wall ($t \simeq 0$) as predicted by $\ddot{b}_1(t)\varphi_j^2/2$ in (10) (is indiscernible thanks to the excellent jitter performance of the M-sequence device.

The trace $b_2(t, T)$ represents the time-variable impulse response of the target for the aspect angles $\varphi = 0°$ (walk towards the antenna) and $\varphi = 180°$ (walk away from the antenna) shifted by the roundtrip time at the related position of the person. To separate coarse and fine motion, we first determine the roundtrip time of the target by estimating the pulse position $t_P(T)$ of the backscattered signal as a function of the observation time T. As already mentioned above, this cannot be done uniquely. For demonstration purposes, we have estimated the time position of the pulse peak $t_{P,max}$ and energetic pulse centre $t_{P,2}$ (see (2) and Fig. 5*d*; note that the maximum position is shifted by 0.5 m for reasons of better visibility). As expected, both approaches show fluctuations, which are caused by the shape variations of the pulses because of the gait of the person. Since the energetic centre is less sensitive to the pulse shape, we have used these data for further processing. The time-dependent pulse positions

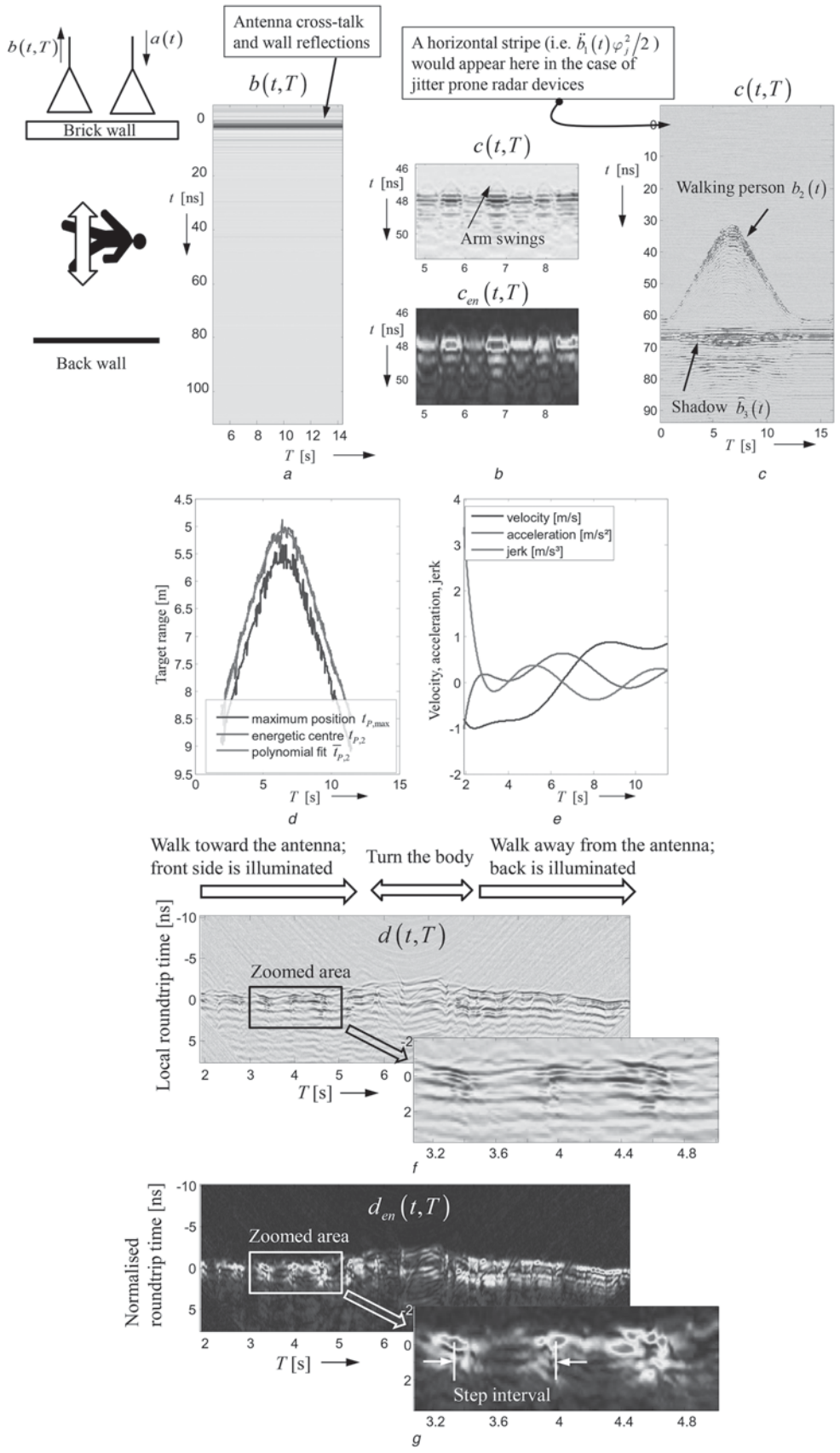

Fig. 5 *Backscattering of a walking human*

a Test arrangement and radar data after impulse compression (baseband M-sequence device (0, …, 3 GHz)double rigid horn DRH10; operational band: 0.7–3 GHz)
b Radargram section of a person walking on the spot (background is removed)
c Radargram of walking person (background is removed)
d Target distance estimated from the roundtrip time of flight
e Higher-order motion components
f and *g* Time aligned target response (*f* – actual signals; *g* – envelope)

doi: 10.1049/iet-rsn.2014.0214

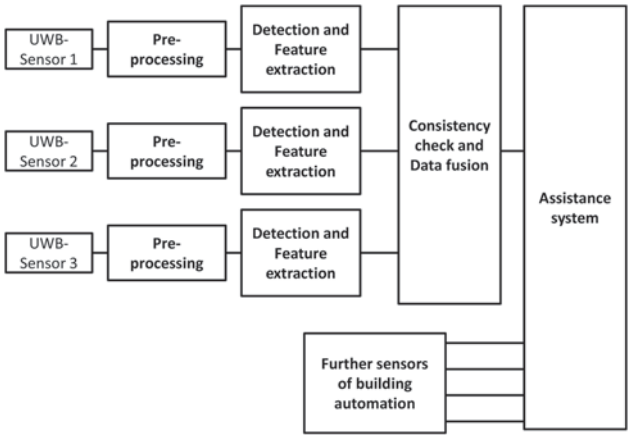

Fig. 6 *Data flow in the sensor network*

$t_{P,2}(T)$ were smoothed (e.g. by polynomial fitting via Savitzky–Golay-filter or any other method) leading to $\bar{t}_{P,2}(T)$, which we consider as the roundtrip time of the target. From this, we yield the target range

$$r(T) = \left|\boldsymbol{r}_A - \boldsymbol{r}_T\right| = \frac{1}{2} c_0 \bar{t}_{P\,2}(T) \tag{14}$$

and the higher 'global' motion components as range velocity v_r, range acceleration a_r, range jerk j_r etc. as illustrated in Fig. 5*e*

$$v_r(T) = \frac{\boldsymbol{v} \cdot \left(\boldsymbol{r}_A - \boldsymbol{r}_T\right)}{\left|\boldsymbol{r}_A - \boldsymbol{r}_T\right|} = \frac{\mathrm{d}r}{\mathrm{d}T};\ a_r(T) = \frac{\mathrm{d}^2 r}{\mathrm{d}T^2};\ j_r(T) = \frac{\mathrm{d}^3 r}{\mathrm{d}T^3} \tag{15}$$

whose patterns may also be characteristic for the gait of a person. (Note that range acceleration and range jerk are no simple projections of the acceleration or jerk vector onto the range vector as in the case of the range velocity.)

To analyse the fine motion of the body, the coarse motion and the divergence of the sounding waves have to be removed from the time-variant IRF $c(t, T)$. This is done by time alignment and amplitude normalisation according to

$$d(t,\ T) = c\left(t - \bar{t}_{P,2}(T),\ T\right)\ r^2(T) \tag{16}$$

as exemplified in Figs. 5*f* and *g*. $d(t, T)$ represents the aspect angle-dependent and time-variant IRF of a walking person. It provides the rhythm of the steps as well as their lengths by assigning the step interval to the target range in Fig. 5*d* (e.g. the indicated step interval in Fig. 5*g* results from a step of about 0.5 m of length). We can also observe the different signal pattern for the illumination of the front of the person ($T < 6$ s) and the back ($T > 7$ s), which well coincides with the results shown in Fig. 4*b*.

5 Vitality capturing for home health monitoring

As we have seen in the previous section, there is a multifaceted interaction between the human body and UWB-radar waves, which can be exploited for monitoring the vitality of seniors in their home. To check the performance of the M-Sequence-UWB-sensors and to gain practical experience with such approaches, realistic experiments in strong multi-path environments have been conducted. For that purpose, we equipped some apartments of seniors with a network of three UWB-sensors and monitored the life and daily routine of the resident for a month. The sensors, which were operating in the ECC-band (Fig. 2*c*) were housed in boxes and positioned in the corners of the apartment at a height of about 1.2 m (compare Fig. 7 left). The beamwidth of the antenna was about 90° so that the whole apartment was illuminated. All sensors were working continuously. A host computer collected the data and provided remote access via Internet for data transfer and system check. The clock rate f_0 of the three UWB-devices was slightly different so that they did

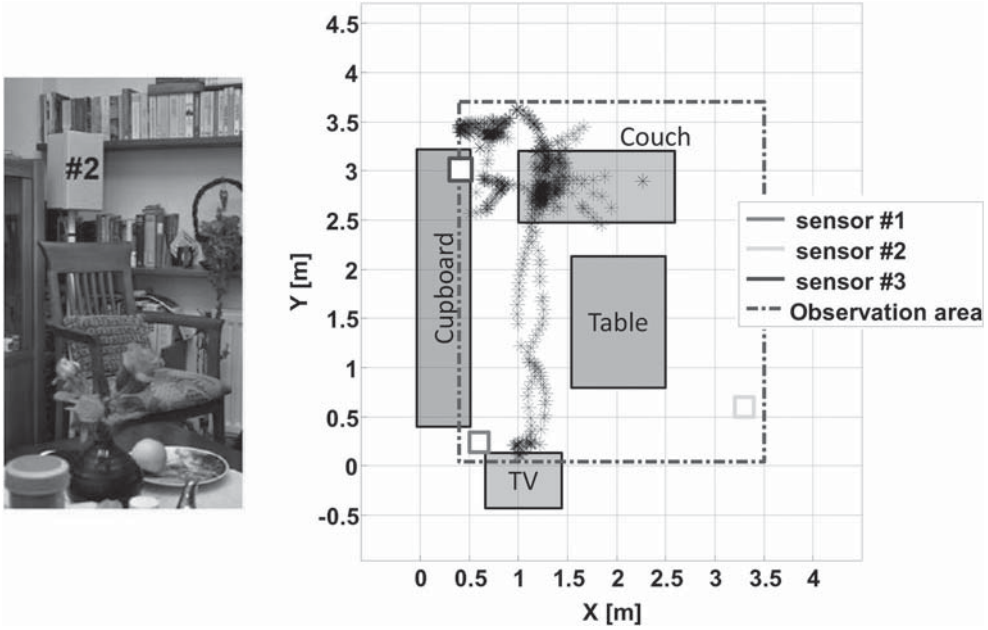

Fig. 7 *Survey of the motion activity of a volunteer in his living room*
Stars in the right-hand graphic represent a 5 min section of a motion profile

not interfere with each other since the sounding signals were mutually de-correlated.

The coarse structure of the data flow of the network is summarised in Fig. 6. The UWB sensors collect the data. The pre-processing stage averages synchronously the data, and performs the impulse compression as well as the background removal. The following processing steps include the target detection (based on a constant false alarm rate (CFAR)-approach) and the extraction of a feature set (range, range velocity, step interval, step size, short-time variance of the target response, features of the $F(T_1, T_2)$-signature, breathing rate and many more). Then, the data gained individually from each sensor are fused and checked for consistency. The consistency check rejects false detections as they may appear if the shadow of the target is quite strong but the target reflection is very weak. Finally, a human-centred assistance system [1], which combines a predictive situation recognition based on probabilistic methods with regulatory interventions through intelligent agents, is aimed to recognise a critical situation and to initiate relief measures.

The strategy to extract vitality signs from the radar data is hierarchically organised depending on the strength of discovered motion, that is, the related algorithms are intended to be activated in descending order if the motion activity decreases:

1. *Two or more people are in the apartment:* The data processing is stopped since a second person can immediately help in the case of an incident.
2. *The resident is alone and walks through the apartment:* The position of the person is tracked from the radar signals. An assistance system uses these data to learn the geometric structure of the apartment and the daily routine of the senior. In the case of any abnormality, the assistance system may initiate adequate activities for help.
3. The gait can be analysed, and its pattern may serve as indicator of health problems (compare Fig. 5).
4. If the senior is sitting on a chair or sleeping in the bed, the chest movement may be registered which indicates his breathing activity (compare Fig. 9). If a motionless body (showing only breathing) is observed away from the

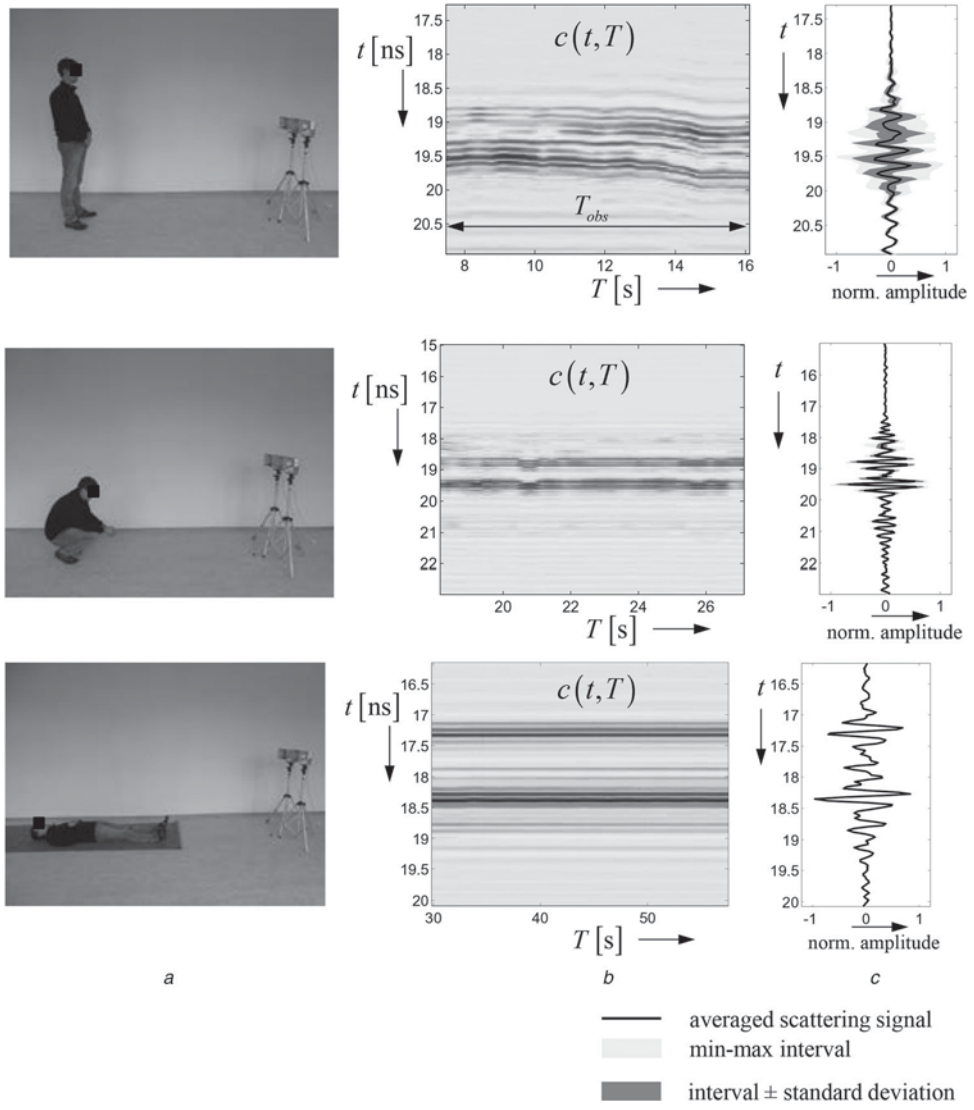

Fig. 8 *Backscattered signal and its fluctuations for a person in different postures (M-sequence radar 12 GHz bandwidth; double rigid horn DRH10). All signals are normalised to the maximum value*

a Photograph of the measurement situation
b Radargram after removal of static background
c Average signal and fluctuation intervals during the observation interval T_{obs}

doi: 10.1049/iet-rsn.2014.0214

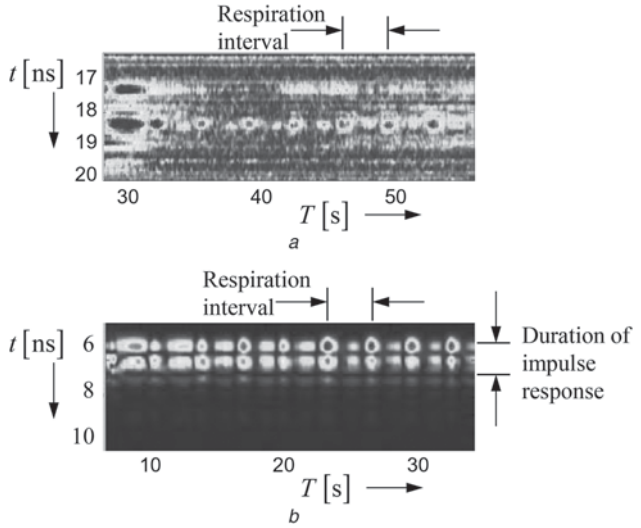

Fig. 9 *Breathing pattern of a person*

a Lying on the floor (radar data from Fig. 8)
b Sitting in a chair (captured with a device corresponding to Fig. 2*c*). The radargrams represent the envelope of the radar data after a second background removal, that is, $c(t, T) - \overline{c(t, T)}|_T$

position of resting furniture, an incident (e.g. a fall) may have happened and will be notified by the assistance system.
5. In the case of a fall, the aspect angle of the radar sensors takes on abnormal values leading to an abnormal shape of the time-variant target IRF and a low short-time variance, which can also be taken as indicator for a critical situation (compare Fig. 8*c*).

The last three figures of this paper shall show some simple examples to illustrate the procedure of capturing information about the vitality of the resident and of recognising critical situations such as a fall. Fig. 7 demonstrates the monitoring of the daily routine of the senior. For the sake of clarity, we only show a short interval of 5 min duration during which the person was moving from the couch to the TV and back. After the above-mentioned consistency check, we determined the position of the person in 1 s intervals based on the roundtrip time provided by the sensors via trilateration [17] and smoothing by α–β-tracking [18].

Note that the individual sensors 'see' the person from different aspect angles leading to range errors (compared with the idealised case of a point target) in the order of the body radius. Hence, we have to respect position errors in the order of the cross-section of the body. Simultaneously to the target location, three feature sets (one from each sensor) of the fine motion may be calculated as illustrated in the previous section. From the target position and the direction of walking, the aspect angle of each sensor can be determined, which allows a better assignment of the fine motion features.

If the movement comes to a halt (i.e. the person is standing still, cowering or lying), the radar processing is aimed to discover the micro-motions of the body as illustrated in Figs. 8 and 9. Fig. 8 compares the micro-motions generated by the body for different postures. As we can observe, the variance of the backscattered signals becomes only small (tending to the noise of the radar system) if the body is fixed by a rigid structure (e.g. chair, bed and floor of the apartment), so that the vestibular organ does not need to control the body position. Hence, if a low variance is detected in $c(t, T)$ over several minutes at locations offside a chair or a bed, there is a high probability of a fall and of an unconsciousness of the habitant. In that case, a second background removal is applied to $c(t, T)$ using a sliding integration window (compare (6) of a shorter time T_a (about half a minute)).

The result is shown in Fig. 9. We can find a periodic signature which is provoked from respiration-induced body motions. Owing to the unfavourable aspect angle in the case of the lying person, the signal magnitude is quite weak. Moreover, with increasing distance from the antenna, the 'breathing' magnitude vanishes in noise so that some enhancement techniques must be used to recover it (see [19] for details). In close proximity to the antenna, even the heart motion can be detected and separated from the respiration motion [20, 21].

6 Summary

Registration of vital activities by radar refers to the capturing and tracking of body displacements and the temporal variation of the body shape. The effect of these variations on the radar signals is often quite weak, and their detection is in 'competition' with the strong reflections from static objects. Paragraph 2 investigates the major effects which limit the detection of weak moving targets in a strong multi-path environment. UWB M-sequence devices meet very well the conditions for sensitive target detection in a harsh multi-path environment because of their high temporal stability. Electromagnetic wave scattering by the human body is multifaceted and provides many options to extract vitality signs of the human or information about his current physical situation. Laboratory and long-term experiments in apartments of seniors have shown the feasibility and appropriateness of the method if the radar data are used by assistance systems for the automatic release of measures to help or assist the senior in the case of an incident.

The long-term experiments were done with modified M-sequence devices whose implementation effort is comparable with that of simple Doppler- or FMCW-radars. So far, the long-term tests have been based solely on unipolar measurements. To increase the reliability of target detection (e.g. prevention of scattering notches – see Figs. 4 and 5) and to provide even more features, polarimetric measurements are recommended and will be investigated in future work.

7 Acknowledgments

This work was supported by the projects AAL@Home (German Federal Ministry of Education and Research) and HaLoS (priority programme SPP 1202 of the German Research Foundation). The authors appreciate the valuable contributions made by M. Grimm, Dr. M. Helbig, M. Kmec, R. Mueller, P. Rauschenbach, K. Schilling and Dr. R. Zetik for sensor development, measurement assistance and helpful discussion as well as ILMsens for providing UWB PN-devices to perform the experiments.

8 References

1 Busch, B.H., Kujath, A., Witthöft, H., Welge, R.: 'Preventive emergency detection based on the probabilistic evaluation of distributed, embedded sensor networks', in Wichert, R., Eberhardt, B. (Eds.): 'Ambient assisted living', (Springer, 2011), pp. 159–179
2 Cuddihy, P.E., Yardibi, T., Legenzoff, Z.J., *et al.*: 'Radar walking speed measurements of seniors in their apartments: technology for fall prevention'. 2012 Annual Int. Conf. of the IEEE presented at the Engineering in Medicine and Biology Society (EMBC), 2012
3 Palmer, J.W., Bing, K.F., Sharma, A.C., Perkins, J.B.: 'Exploitation of radar Doppler signatures for gait analysis'. 2012 Conf. Record of the

46th Asilomar Conf. on presented at the Signals, Systems and Computers (ASILOMAR), 2012
4 Zakrzewski, M., Vanhala, J.: 'Separating respiration artifact in microwave Doppler radar heart monitoring by independent component analysis'. Presented at the Sensors, 2010 IEEE, 2010
5 Zetik, R., Jovanoska, S., Thoma, R.: 'Simple method for localisation of multiple tag-free targets using UWB sensor network'. 2011 IEEE Int. Conf. on Ultra-Wideband (ICUWB), 2011, pp. 268–272
6 Porcino, D., Sachs, J., Zetik, R., Ward, A.: 'UWB ranging', in d. Benedetto, M.G., Kaiser, T., Molisch, A., Oppermann, I., Politano, C., Porcino, D. (Eds.): 'UWB communication systems a comprehensive overview' (Hindawi Publishing Corporation, New York, 2006), pp. 411–446
7 Sachs, J.: 'On the range estimation by UWB-radar'. Presented at the IEEE Int. Conf. on Ultra-Wideband (ICUWB), Paris (France), 2014
8 Sachs, J.: 'Handbook of ultra-wideband short-range sensing – theory, sensors, applications' (Wiley-VCH, Berlin, 2012)
9 Sachs, J., Herrmann, R., Kmec, M.: 'Time and range accuracy of short-range ultra-wideband pseudo-noise radar', *Appl. Radio Electron.*, 2013, **12**, pp. 105–113
10 Sachs, J., Kmec, M., Fritsch, H.C., *et al.*: 'Ultra-wideband pseudo-noise sensors', *Appl. Radio Electron.*, 2013, **12**, pp. 79–88
11 Müller, R., Herrmann, R., Wollenschläger, F., Schulz, A., Hein, M.A., Thomä, R.: 'A compact ECC-band horn antenna for remote monitoring of vital signs at home environments'. Presented at the EuCAP 2013, Gothenburg (Sweden), 2013
12 Cohn, M., Lempel, A.: 'On fast M-sequence transforms (Corresp.)', *IEEE Trans. Inf. Theory*, 1977, **23**, pp. 135–137
13 Kmec, M.: 'Monolithically integration of m-sequence-based sensor head', in Sachs, J. (Ed.): 'Handbook of ultra-wideband short range sensing' (Wiley-VCH, Weinheim, Germany, 2012)
14 Herrmann, R.: 'M-sequence based ultra-wideband radar and its application to crack detection in salt mines' (Faculty of Electrical Engineering and Information Technology, Ilmenau University of Technology (Germany), Ilmenau, 2011)
15 Smith, G.E., Ahmad, F., Amin, M.G.: 'Micro-Doppler processing for ultra-wideband radar data'. Presented at the Proc. SPIE 8361, Radar Sensor Technology XVI, 2012, 83610 L 10 pages
16 Chen, V.C., Tahmoush, D., Miceli, W.J. (Eds.): 'Radar micro-Doppler signature – processing and applications' (IET Radar Series, The Institution of Engineering and Technology, London, 2014)
17 Zetik, R.: 'UWB localization'. in Sachs, J. (Ed.): 'Handbook of ultra-wideband short-range sensing: theory, sensors, applications', (Wiley VCH, Weinheim, 2012)
18 Chiou, Y.S., Wang, C.L., Yeh, S.C.: 'Reduced-complexity scheme using alpha–beta filtering for location tracking', *IET Commun.*, 2011, **5**, pp. 1806–1813
19 Sachs, J., Helbig, M., Herrmann, R., Kmec, M., Schilling, K., Zaikov, E.: 'Remote vital sign detection for rescue, security, and medical care by ultra-wideband pseudo-noise radar'. Ad Hoc Networks, 2012
20 Kosch, O., Thiel, F., Schwarz, U., Hein, M., Seifert, F.: 'UWB cardiovascular monitoring for enhanced magnetic resonance imaging', in Sachs, J. (Ed.): 'Handbook of ultra-wideband short-range sensing: theory, sensors, applications' (Wiley-VCH, Weinheim, 2012)
21 Kosch, O., Thiel, F., Seifert, F., Sachs, J., Hein, M.A.: 'Motion detection in-vivo by multi-channel ultrawideband radar'. 2012 IEEE Int. Conf. on Presented at the Ultra-Wideband (ICUWB), 2012

9 Appendix

9.1 Annex: synchronous average of jittered waveform

We assume a deterministic signal $x(t)$ which is periodically repeated and whose sampling points are jittered by $\Delta\tau_j(t)$, with $t = m\Delta t$ representing the intended sampling time. For the sake of shortness, we dispense with t as argument of $\Delta\tau_j$ in what follows. We consider the jitter as ergodic random process with PDF $p_{\Delta\tau_j}(t')$, in which t' is a difference time referred to the intended sampling time points. The jitter events of the individual data samples are supposed to be uncorrelated.

The averaged signal is a random process too, which we may write as

$$\underset{\sim}{\bar{x}}(t) = \frac{1}{N}\sum_{n=0}^{N-1} x\left(t + \Delta\underset{\sim}{\tau}_{j,n}\right) \tag{17}$$

To calculate the expected value of the averaged signal, we use Taylor-series expansion, whereat $\overset{(\nu)}{x}(t)$ means ν-fold derivation by time t (see (18)). Using $E\{\Delta\underset{\sim}{\tau}_j^{\nu}\} = \int_{-\infty}^{\infty} t'^{\nu} p_{\Delta\tau_j}(t')dt'$, (18) may be rewritten as (see (19)). The variance of the averaged value results from (see (20) at the bottom of the next page). One of the two terms is already known from (19) and for the still unknown term, we expand $x(t)$ in a Taylor series and rewrite its square as a Cauchy product

$$\begin{aligned} E\left\{\left(\underset{\sim}{x}(t)\right)^2\right\} &= E\left\{\left(\sum_{\nu=0}^{\infty}\frac{1}{\nu!}\overset{(\nu)}{x}(t)\Delta\underset{\sim}{\tau}_j^{\nu}\right)^2\right\} \\ &= E\left\{\sum_{n=0}^{\infty}\sum_{a+b=n}\frac{1}{a!}\overset{(a)}{x}(t)\Delta\underset{\sim}{\tau}_j^{a}\frac{1}{b!}\overset{(b)}{x}(t)\Delta\underset{\sim}{\tau}_j^{b}\right\} \\ &= \sum_{n=0}^{\infty}\sum_{a+b=n}\frac{1}{a!}\overset{(a)}{x}(t)\frac{1}{b!}\overset{(b)}{x}(t)E\left\{\Delta\underset{\sim}{\tau}_j^{a+b}\right\} \end{aligned} \tag{21}$$

$$\begin{aligned} E\{\underset{\sim}{\bar{x}}(t)\} &= E\left\{\frac{1}{N}\sum_{n=0}^{N-1}x\left(t+\Delta\underset{\sim}{\tau}_{j,n}\right)\right\} = E\left\{\frac{1}{N}\sum_{n=0}^{N-1}\sum_{\nu=0}^{\infty}\frac{\overset{(\nu)}{x}(t)}{\nu!}\Delta\underset{\sim}{\tau}_{j,n}^{\nu}\right\} \\ &= \sum_{\nu=0}^{\infty}\frac{\overset{(\nu)}{x}(t)}{\nu!}E\left\{\Delta\underset{\sim}{\tau}_j^{\nu}\right\} \\ &\text{since } \frac{1}{N}\sum_{n=0}^{N-1}E\left\{\Delta\underset{\sim}{\tau}_{j,n}^{\nu}\right\} = E\left\{\Delta\underset{\sim}{\tau}_j^{\nu}\right\} \quad \text{because of to ergodicity of jitter} \end{aligned} \tag{18}$$

$$\begin{aligned} E\left\{\underset{\sim}{\bar{x}}(t)\right\} &= \sum_{\nu=0}^{\infty}\frac{\overset{(\nu)}{x}(t)}{\nu!}\int_{-\infty}^{\infty}t'^{\nu}p_{\Delta\tau_j}(t')\,\mathrm{d}t' = \int_{-\infty}^{\infty}\left(\sum_{\nu=0}^{\infty}\frac{\overset{(\nu)}{x}(t)}{\nu!}t'^{\nu}\right)p_{\Delta\tau_j}(t')\,\mathrm{d}t' \\ &= \int_{-\infty}^{\infty}x(t+t')p_{\Delta\tau_j}(t')\,\mathrm{d}t' \text{ since } x(t+t') = \sum_{\nu=0}^{\infty}\frac{\overset{(\nu)}{x}(t)}{\nu!}t'^{\nu} \\ &= x(t) * p_{\Delta\tau_j}(t) \end{aligned} \tag{19}$$

doi: 10.1049/iet-rsn.2014.0214

The summation indices a, b result from all variations of a and b whose sum equals n. Expressing again the expected value by the PDF of the jitter, taking back Taylor series and Cauchy product, we yield

$$\begin{aligned} E\left\{\left(\underset{\sim}{x}(t)\right)^2\right\} &= \sum_{n=0}^{\infty}\sum_{a+b=n}\frac{1}{a!}\overset{(a)}{x}(t)\frac{1}{b!}\overset{(b)}{x}(t)\int_{-\infty}^{\infty}t'^{a+b}p_{\Delta\tau_j}(t')\,\mathrm{d}t' \\ &= \int_{-\infty}^{\infty}\sum_{n=0}^{\infty}\sum_{a+b=n}\frac{1}{a!}\overset{(a)}{x}(t)\frac{1}{b!}\overset{(b)}{x}(t)t'^{a+b}p_{\Delta\tau_j}(t')\,\mathrm{d}t' \\ &= \int_{-\infty}^{\infty}x(t-t')^2p_{\Delta\tau_j}(t')\,\mathrm{d}t' \\ &= x^2(t)*p_{\Delta\tau_j}(t) \end{aligned} \tag{22}$$

so that we find from (19), (20) and (22)

$$\mathrm{var}\left\{\underset{\sim}{\bar{x}}(t)\right\} = \frac{1}{N}\left(x^2(t)*p_{\Delta\tau_j}(t) - \left(x(t)*p_{\Delta\tau_j}(t)\right)^2\right) \tag{23}$$

Assuming Gaussian distributed jitter, that is, $p_{\Delta\tau_j}(t') = \mathrm{e}^{-(1/2)\left(t'/\varphi_j\right)^2}/\sqrt{2\pi}\varphi_j$, (19) and (23) may be approximated as ($n!!$ – double factorial)

$$\begin{aligned} E\left\{\underset{\sim}{\bar{x}}(t)\right\} &= \sum_{n=0}^{\infty}\frac{\overset{(2n)}{x}(t)}{(2n)!!}\varphi_j^{2n} \\ &= x(t) + \frac{1}{2}\ddot{x}(t)\varphi_j^2 + \frac{1}{8}\ddot{\ddot{x}}(t)\varphi_j^4 + \cdots \end{aligned} \tag{24}$$

and (see (25)). To obtain (24) and (25) from (19) and (23), we have exploited Taylor-series expansion and the identities

$$\int_{-\infty}^{\infty}\tau^n\mathrm{e}^{-(1/2)\left(\tau/\varphi_j\right)^2}\,\mathrm{d}\tau = \begin{cases} 0, & n \text{ odd} \\ \sqrt{2\pi}(n-1)!!\varphi_j^{n+1}; & n \text{ even} \end{cases}$$

$$\frac{\mathrm{d}^n}{\mathrm{d}t^n}x^2(t) = \sum_{k=0}^{n}\binom{n}{k}\frac{\mathrm{d}^{n-k}}{\mathrm{d}t^{n-k}}x(t)\frac{\mathrm{d}^k}{\mathrm{d}t^k}x(t) = \sum_{k=0}^{n}\binom{n}{k}\overset{(n-k)}{x}(t)\overset{(k)}{x}(t)$$

$$\begin{aligned} \mathrm{var}\left\{\underset{\sim}{x}(t)\right\} &= \mathrm{var}\left\{\frac{1}{N}\sum_{n=0}^{N-1}x\left(t+\Delta\underset{\sim}{\tau}_{j,n}\right)\right\} \\ &= \frac{1}{N}\,\mathrm{var}\left\{x\left(t+\Delta\underset{\sim}{\tau}_j\right)\right\} \text{ since } \mathrm{cov}\left\{x\left(t+\Delta\underset{\sim}{\tau}_{j,n}\right),\, x\left(t+\Delta\underset{\sim}{\tau}_{j,m}\right)\right\} = 0 \\ &= \frac{1}{N}\left(E\left\{\left(x\left(t+\Delta\underset{\sim}{\tau}_j\right)\right)^2\right\} - E^2\left\{x\left(t+\Delta\underset{\sim}{\tau}_j\right)\right\}\right) \end{aligned} \tag{20}$$

$$\begin{aligned} \mathrm{var}\left\{\underset{\sim}{\bar{x}}(t)\right\} &= \frac{1}{N}\left(\sum_{n=0}^{\infty}\frac{1}{(2n)!!}\left(\sum_{k=0}^{2n}\binom{2n}{k}\overset{(2n-k)}{x}(t)\overset{(k)}{x}(t)\right)\varphi_j^{2n} - \left(\sum_{n=0}^{\infty}\frac{\overset{(2n)}{x}(t)}{(2n)!!}\varphi_j^{2n}\right)^2\right) \\ &= \frac{1}{N}\left(\dot{x}^2(t)\varphi_j^2 + \frac{1}{4}\ddot{x}^2(t)\varphi_j^4 + \cdots\right) \end{aligned} \tag{25}$$